Polymer 50 (2009) 4944–4949

Contents lists available at ScienceDirect

Polymer

journal homepage: www.elsevier.com/locate/polymer

Phase behavior of poly(3-alkylthiophene)/polystyrene blends

Youngmin Lee [a], Jin Kon Kim [a,*], Chu-Han Chiu [b], Yi-Kang Lan [b], Ching-I Huang [b,**]

[a] National Creative Research Initiative Center for Block Copolymer Self-Assembly, Department of Chemical Engineering and Polymer Research Institute, Pohang University of Science and Technology, San 31, Hyo-ja dong, Pohang, Kyungbuk 790-784, Republic of Korea
[b] Institute of Polymer Science and Engineering, National Taiwan University, Taipei 10617, Taiwan

ARTICLE INFO

Article history:
Received 20 April 2009
Received in revised form
28 July 2009
Accepted 9 August 2009
Available online 13 August 2009

Keywords:
Phase behavior
P3AT/PS blend
Monte Carlo simulation

ABSTRACT

Phase diagrams of blends consisting of poly(3-*n*-alkylthiopene) having four different *n*-alkyl side chain lengths ($n = 4, 6, 8, 12$) and polystyrene (PS) were obtained by turbidity measurement. All of the P3AT/PS blends employed in this study exhibited the upper critical solution temperature (UCST) type phase behavior. From $n = 4$ [poly(3-butylthipene)] to $n = 6$ [poly(3-hexylthipene)], the miscibility between P3AT/PS blends decreased, but with further increase in the value of *n*, the miscibility increased. Thus, the miscibility of the P3HT/PS blend becomes the least among four blend pairs. This interesting phase behavior depending on *n* was successfully illustrated via the combination of Monte Carlo simulation and molecular dynamics.

1. Introduction

Poly(3-alkylthiophene) (P3AT) has been extensively used for organic field-effect transistors [1–3], chemical sensors [4,5], and photovoltaic solar cell [6–9] due to its excellent optoelectric properties and good solubility in various kinds of solvents. Recently, many research groups have investigated the blends of P3AT and conventional non-conductive polymers to improve processability and mechanical strength as well as the cost-reduction of the expensive P3AT, while excellent electric and optoelectric properties of P3AT are maintained. For instance, poly(3-hexylthiopene) (P3HT)/polyethylene blend exhibited almost the same charge-carrier-mobility as that of neat P3HT, even when the weight fraction of P3HT in the blend was as small as 0.15 [10]. Also, Yang and coworkers [11] showed that the electric conductivity of poly(3-butylthiophene) (P3BT)/PS blend was higher than that of neat P3BT.

Morphology and phase behavior of the P3AT-containing blends significantly affect electric and optoelectric properties. When the miscibility between P3AT and non-conducting polymer becomes very poor, the conductivity of the blend is small. On the other hand, perfect mixing on a molecular level is not desirable either, because the conductive network of P3AT is not easily formed. Recently, Jaczewska et al. investigated the miscibility between P3AT with various lengths of alkyl chain ($n = 4$, 6, 12) and solvents and calculated the solubility parameter (δ) of P3AT [12]. They found that δ depends on the regioregularity as well as *n*. They also investigated the thin film morphology of P3AT/PS blends [13]. Levon and coworkers studied the miscibility between poly(3-octylthiopene) (P3OT) and poly(ethylene-co-vinylacetate) (EVA) [14]. They experimentally determined the turbidity temperature above which macrophase-separated morphology was observed for two blend compositions (20/80 and 15/85 (wt/wt) P3OT/EVA) and concluded that this blend exhibited lower critical solution temperature (LCST) type phase behavior. However, to the best of our knowledge, phase diagrams of the blends of P3AT with various *n* and non-conductive polymers such as polystyrene have not been obtained experimentally. To achieve this objective, the lower molecular weights (2000–3000) of P3AT should be synthesized. When commercially available P3ATs with larger molecular weights ($\sim$20000) were blended with PS, one could not obtain the turbidity temperature experimentally before the thermal degradation temperature.

In this work, we experimentally obtained the phase diagrams of the blends consisting of P3AT with four different values of *n* ($n = 4$, 6, 8, 12) and PS by using turbidity measurement. Interestingly, with increasing *n*, the miscibility of P3AT and PS did not monotonically increase (or decrease); rather, the miscibility of P3HT ($n = 6$)/PS blend became the least. To illustrate this interesting phase behavior depending on *n*, we estimated the Flory-Huggins interaction parameter (χ) between P3AT and PS by using the combination of Monte Carlo simulation and molecular dynamics (MD). This

* Corresponding author. Tel.: +82 54 279 2276; fax: +82 54 279 8298.
** Corresponding author.
E-mail addresses: jkkim@postech.ac.kr (J.K. Kim), chingih@ntu.edu.tw (C.-I. Huang).

0032-3861/$ – see front matter © 2009 Elsevier Ltd. All rights reserved.
doi:10.1016/j.polymer.2009.08.012

molecular approach considers the actual force fields; thus it provides a better understanding of atomic level interactions responsible for the immiscibility between polymer–polymer and polymer–solvent pairs [15–18]. For simplicity, we compute the pair-wise interaction energies and the spatial coordination numbers between 3AT monomer and styrene dimer, which allows us to obtain χ between P3AT and PS. Because our simulated systems consist of monomer or dimer type, the calculated χ does not include the entropic contribution; thus it does not correspond to the "true" interaction parameter [17]. However, it still includes the specific interactions associated with dissimilar groups in an atomic level. We found that the estimated χ depending on the alkyl chain length in the 3AT monomers was consistent with the measured miscibility between PS and P3AT.

2. Experimental section

2.1. Materials

Polystyrenes (PS-4, PS-5) were purchased from Polymer Source, Inc. The weight-average molecular weight (M_w) and the polydispersity index (PDI = M_w/M_n, where M_n is the number-average molecular weight) are 3700 and 1.06 for PS-4, and 5100 and 1.08 for PS-5. Various P3ATs with four different values of n ($n = 4, 6, 8, 12$) were polymerized by using 2-bromo-3-alkylthiophene according to the methods reported in the literature [19,20]. Diisopropylamine (Aldrich, 99.5+%) was freshly distilled before use. Tetrahydrofuran (THF) was first stirred with CaH_2, and distilled. All reagents except those were used without further purification. Typical polymerization of P3HT was performed as follows. Freshly distilled diisopropylamine (67.0 mmol, 6.79 g) and n-butyl lithium (63.7 mmol, 32.0 ml) were dissolved in dry THF at −78 °C and mixed for 5 min. Then, 2-bromo-3-hexylthiophene (67.0 mmol, 16.30 g) was added to the above mixture and stirred for 1 h. Anhydrous $ZnCl_2$ (67.0 mmol, 9.13 g) was added and stirred for 1 h. The mixture was warmed to 0 °C and Ni(dppp)Cl_2 was added and polymerized at this temperature for 20 min. Finally, the product was quenched with methanol. The polymerization time and temperature were varied for different P3ATs: 10 min at 0 °C for P3BT ($n = 4$), 30 min at room temperature for P3OT ($n = 8$), and 20 min at 40 °C for poly(3-dodecylthiophene) (P3DDT, $n = 12$).

The molecular weights of as-synthesized P3ATs are very high; thus we could not use as-synthesized P3ATs for the observation of the turbidity temperature for P3AT/PS blend. Furthermore, the polydispersity index (PDI) of as-synthesized P3ATs was rather broad (~1.4). Thus, we performed the fractionation of as-synthesized P3ATs by sequential Soxhlet extraction with methanol, hexane, dichloromethane (DCM), THF and chloroform. In this study, the hexane-extracted was used for P3HT and P3OT, while DCM-extracted P3BT was used. On the other hand, for P3DDT, we used double fractionations to obtain similar molecular weights of other three P3ATs. Namely, as-synthesized P3DDT was first fractionated by hexane. Then, the hexane-fractionated P3DDT was again fractionated by using hexane/acetone (50/50 v/v) mixture.

2.2. Characterization

Gel permeation chromatograms (GPC) (Waters) were obtained by using THF as the eluent, and the molecular weight was calibrated based on PS standards. MALDI-TOF (Bruker) experiment was performed with using dithranol matrix without any salt. Molecular characteristics of P3ATs employed in this study are given in Table 1. It is seen that the weight-average molecular weight (M_w) measured by MALDI-TOF of all the P3ATs are 20–30% smaller than that measured by GPC with PS standards. This difference is well consistent with the result given in Ref. [21]. The PDI of four P3ATs determined by MALDI-TOF is relatively narrow ($\leq$1.12), thus all of P3ATs are assumed to be nearly monodisperse. For the calculation of the Flory–Huggins interaction parameter based on the binodal curves, the values of M_w measured by MALDI-TOF were used. Melting points (T_m) of P3ATs were obtained by differential scanning calorimetry (DSC) (Perkin Elmer) obtained during second heating at a rate of 10 °C/min. The regioregularity of P3AT was obtained from the area ratio of the peak at 2.8 ppm to the peaks appearing at 2.5–3.2 ppm in ^{1}H nuclear magnetic resonance (NMR) spectrum (Bruker) [22]. The values of T_m and the regioregularity of P3ATs are also given in Table 1.

Table 1
Molecular characteristics and the regioregularity of P3AT and PS employed in this study.

	M_w (kg/mol) by GPC	M_w (kg/mol) by MALDI-TOF	M_w/M_n by MALDI-TOF	T_m (°C)	Regioregularity (%)
P3BT	3.6	2.5	1.11	182	80
P3HT	3.1	2.4	1.12	85	79
P3OT	2.9	2.3	1.11	64	75
P3DDT	3.3	2.3	1.09	40	76

2.3. Turbidity temperature measurement

P3AT/PS blends with various blend compositions were dissolved into toluene and solution-cast on a cover glass. The solvent was completely removed by using a vacuum oven at room temperature until a constant weight was achieved. The blend was annealed under vacuum for 12 h at temperatures above T_m of each P3AT (200 °C for P3BT and 150 °C for other three P3ATs). The turbidity temperature (T_b) of each blend composition was first estimated by the threshold temperature above which macrophase-separated structures were not observed under the optical microscope (OM) (Zeiss) with a magnification of 400 upon heating at a rate of 1 °C/min. Once T_b of a specimen was estimated, the exact T_b was determined by OM with a stepwise change of 1 °C near the T_b; thus the maximum error in T_b would be less than ±1 °C. The measured T_b of each blend composition for P3AT/PS pairs was higher than T_m of its P3AT.

3. Theoretical section

To examine the effects of alkyl chain length n on the miscibility between P3AT and PS, we employed Monte Carlo (MC) simulation to compute the pair-wise interaction energies and the spatial coordination numbers, which allow us to calculate the Flory-Huggins interaction parameter χ between P3AT and PS. Here, 3AT monomer and styrene dimer were used because the volume of styrene dimer is typically in the range among the four different 3AT monomers with $n = 4$–12.

We considered two types of the configuration of 3AT monomers. The first one is 'without annealing', i.e., the alkyl side chain in the 3AT monomer was artificially set to maintain the coplanar zigzag conformation with respect to the thiophene ring. We then employed MC simulation to calculate the Flory-Huggins interaction parameter χ between styrene dimer and each 3AT monomer.

The second one is that 3AT monomer is equilibrated 'with annealing' via the molecular dynamics (MD) simulation with the Dreiding force field. The annealing temperature was first raised from 423 to 800 K at a rate of 38 K/ps, and then quenched to 423 K at the same rate. This annealing cycle was repeated 20 times to ensure that the 3AT monomer was equilibrated. Each 3AT monomer was simulated for 30 times via the similar annealing processes to collect possible structures. Then MC simulation was performed

to obtain the χ value of the equilibrated 3AT monomer and styrene dimer. These values were then averaged by using the Boltzmann method.

The Flory-Huggins interaction parameter χ between a pair of components 1 and 2 was calculated according to the following equation:

$$\chi = \frac{\Delta E_{\mathrm{mix}}}{RT} \tag{1}$$

where ΔE_{mix} is the difference of the average binding energy between similar and dissimilar pairs, and given as:

$$\Delta E_{\mathrm{mix}} = \frac{1}{2}Z_{12}\langle E_{12}\rangle + Z_{21}\langle E_{21}\rangle - \frac{1}{2}Z_{11}\langle E_{11}\rangle + Z_{22}\langle E_{22}\rangle \tag{2}$$

where Z_{ij} and $\langle E_{ij}\rangle$ are the coordination numbers and the average binding energy of a particular i and j pair, respectively. The pairwise interaction energy $\langle E_{ij}\rangle$ was calculated by averaging the results over a large number of configurations (at least 1,000,000) and a probability distribution function $P(E_{ij})$ generated by the MC method with the Boltzmann method:

$$\langle E_{ij}(T)\rangle = \frac{\int dE_{ij}P(E_{ij})E_{ij}\exp\left(\frac{-E_{ij}}{k_BT}\right)}{\int dE_{ij}P(E_{ij})\exp\left(\frac{-E_{ij}}{k_BT}\right)} \tag{3}$$

4. Results and discussion

Fig. 1 gives OM images of 25/75 (wt/wt) and 70/30 (wt/wt) P3HT/PS-1 blends at two temperatures. Dark and bright regions are P3HT and PS phases, respectively. Even though the molecular weights of P3AT and PS were rather small, the macrophase separation occurred. The phase-separated morphology at lower temperatures for 25/75 (wt/wt) blend disappeared completely at 222 °C, while the 70/30 (wt/wt) blend became homogeneous state at 200 °C. We found that the phase transition temperature was thermally reversible. Based on the results in Fig. 1 and the repeated experiments for other compositions, we obtained the phase diagram of P3HT/PS blend, as shown in Fig. 2a. Similarly, we obtained the phase diagrams of other three blend systems ($n = 4$, 8, and 12), as shown in Fig. 2b–d. All blends showed the upper critical solution temperature (UCST) type phase behavior. It is seen in Fig. 2 that at a given molecular weight, the UCST is the highest for P3HT/PS blend, while it is the lowest for P3DDT/PS blend.

To estimate the Flory–Huggins interaction parameter (χ) for each blend, we employed the Flory–Huggins lattice theory. The free energy difference (ΔG_{m}) between the mixing state and phase-separated state is given by [23]:

$$\Delta G_{\mathrm{m}}/(k_BT)V \equiv \frac{\phi_1 \ln\phi_1}{V_1} + \frac{\phi_2 \ln\phi_2}{V_2} + \alpha\phi_1\phi_2 \tag{4}$$

Here, k_B and T are the Boltzmann constant and the absolute temperature, and V is the total system volume. ϕ_i and V_i ($i = 1, 2$) are the volume fraction and the molar volume of component i in the blend. α is given by χ/V_{ref}, in which V_{ref} is the monomeric volume of a reference component; thus the dimension of α is mole/cm^3. In this study, we used the composition and temperature dependence of α [23]:

$$\alpha = a + b/T + c\phi_2 = \alpha_0 + c\phi_2 \tag{5}$$

The chemical potential (μ) of each component is given by [24]:

$$\Delta\mu_1/(k_BTV_1) \equiv \frac{\ln\phi_1}{V_1} + \frac{(1-\phi_1)}{V_1} - \frac{\phi_2}{V_2} + \left[\alpha_0 + \frac{c(1-2\phi_1)}{T}\right]\phi_2^2 \tag{6a}$$

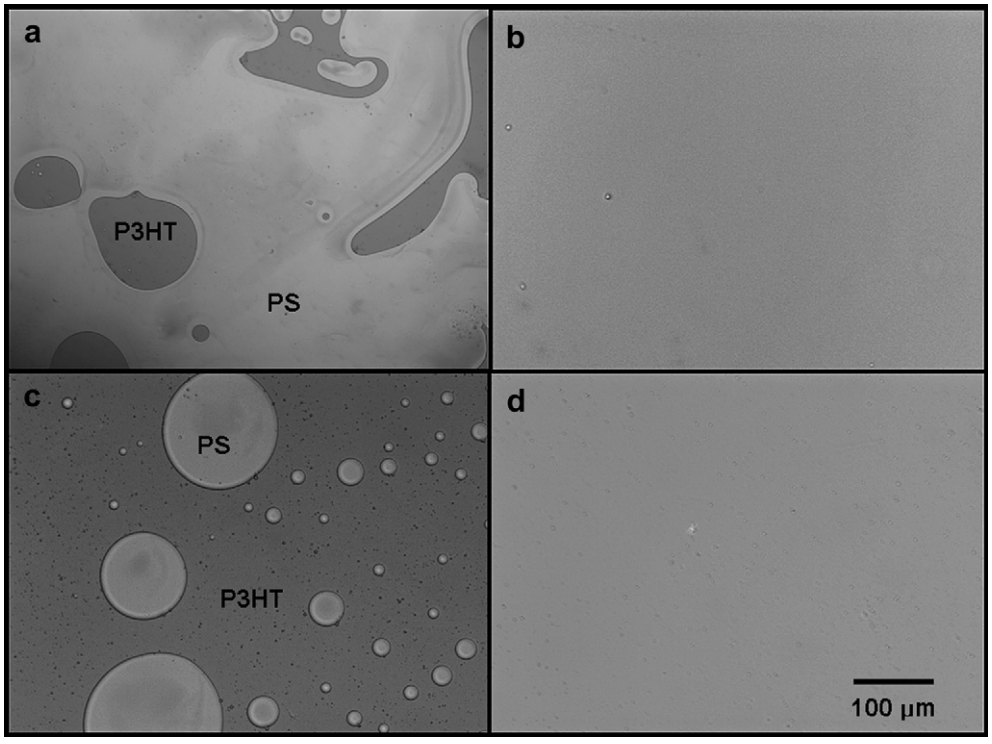

Fig. 1. OM images of 25/75 (wt/wt) P3HT/PS-4 blends (a and b) and 70/30 (wt/wt) P3HT/PS-4 blends (c and d) at two temperatures. (a) 221 °C, (b) 222 °C, (c) 199 °C and (d) 200 °C.

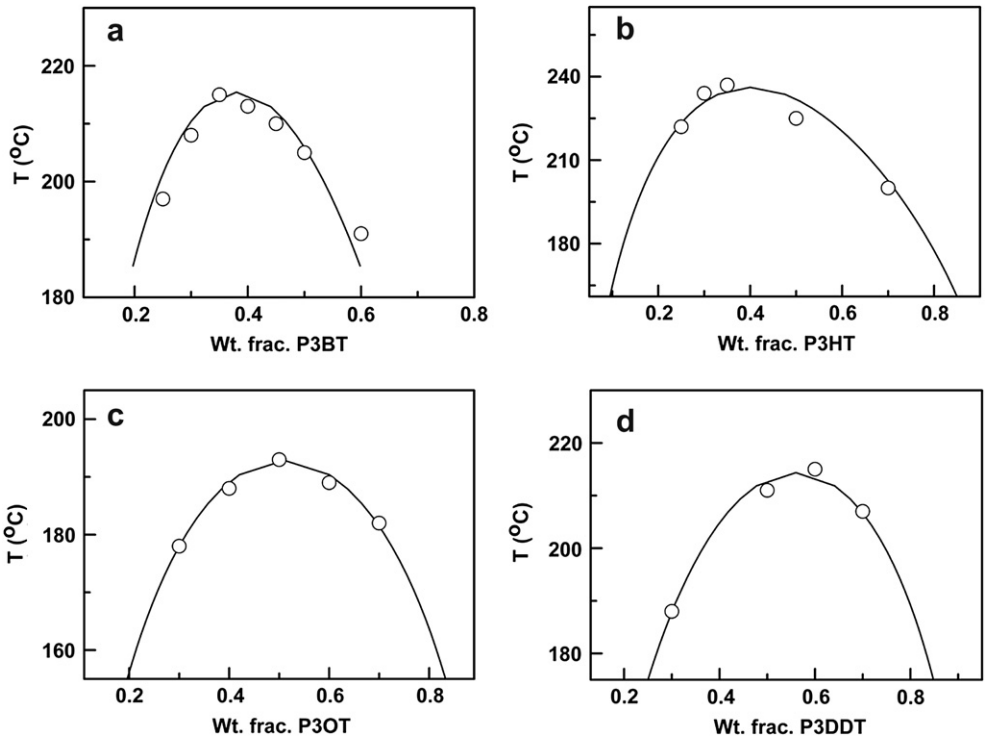

Fig. 2. Phase diagrams of (a) P3BT/PS-5, (b) P3HT/PS-4, (c) P3OT/PS-4, and (d) P3DDT/PS-5. The solid lines are the predicted binodal curves from the Flory–Huggins lattice model with Eq. (10a)–(10d), respectively.

$$\Delta\mu_2/(k_BTV_2) \equiv \frac{\ln\phi_2}{V_2} + \frac{(1-\phi_2)}{V_2} - \frac{\phi_1}{V_1} + \left[\alpha_0 + \frac{2c\phi_2}{T}\right]\phi_1^2 \tag{6b}$$

The binodal curve is easily obtained from the following equations.

$$\Delta\mu_1(\phi_1', \phi_2') \equiv \Delta\mu_1(\phi_1'', \phi_2'') \tag{7a}$$

$$\Delta\mu_2(\phi_1', \phi_2') \equiv \Delta\mu_2(\phi_1'', \phi_2'') \tag{7b}$$

where $\phi_1'(=1-\phi_2')$ and $\phi_1''(=1-\phi_2'')$ represent the volume fraction of component "1" at two separated regions. From Eqs. (6a) into (7a), we have:

$$\alpha_0 \equiv \frac{1}{(\phi_2'')^2-(\phi_2')^2}\left[\frac{\ln[(1-\phi_2')/(1-\phi_2'')]}{V_1} + \left(\frac{1}{V_1}-\frac{1}{V_2}\right) \times(\phi_2'-\phi_2'') + \frac{2c\left[(\phi_2')^3-(\phi_2'')^3\right]}{T}\right] + \frac{c}{T} \tag{8a}$$

Similarly, from Eqs. (6b) and (7b), we obtain

$$\alpha_0 \equiv \frac{1}{(1-\phi_2'')^2-(1-\phi_2')^2}\left[\frac{\ln(\phi_2'/\phi_2'')}{V_2} + \left(\frac{1}{V_1}-\frac{1}{V_2}\right)(\phi_2'-\phi_2'') + \frac{2c\left[\phi_2'(1-\phi_2')^2-\phi_2''(1-\phi_2'')^2\right]}{T}\right] \tag{8b}$$

On the other hand, c in Eq. (5) is given by [24]:

$$c \equiv \frac{T_c}{6}\left[\frac{1}{V_1(1-\phi_{2,c})^2} - \frac{1}{V_2(\phi_{2,c})^2}\right] \tag{9}$$

where T_c and $\phi_{2,c}$ are the critical temperature and volume faction of component 2 (P3AT in this study).

Since ϕ_2' at one phase-separated region is known from the turbidity curve at each turbidity temperature, ϕ_2'' could be obtained from Eq. (8a) and (8b) as follows. First, the range of ϕ_2'' is chosen as from 0 to $\phi_{2,c}$ for $\phi_2'' > \phi_{2,c}$, whereas it is from $\phi_{2,c}$ to 1 for $\phi_2'' < \phi_{2,c}$. Next, α_0 is calculated by both Eq. (8a) and (8b) at all possible values of ϕ_2''. The volume fraction at the other separate-phase (ϕ_2'') is determined as the value where the square of the difference in α_0 calculated from Eq. (8b) and Eq. (8b) becomes zero (or the minimum among all possible values). Once ϕ_2'' is determined, α_0 is calculated from Eq. (8a) (or Eq. (8b)). Finally, the values of a, b, and c in Eq. (5) are obtained from the multiple regression method by using the values of α determined at all of the experimentally determined turbidity temperatures.

We are well aware that when the constituent polymers in the blend are polydisperse, Eq. (6a) and (6b) should be changed; thus the phase diagram (or calculated α) should be different from that of another blend with monodisperse polymer [25,26]. However, since the polydispersity of P3AT is quite narrow (less than 1.12) and not much larger than those of PS-4 and PS-5 employed in this study that are prepared by anionic polymerization, we do not consider the effect of the polydispersity on the phase diagram (thus, α) in this study.

The values of α for four blends calculated from the above procedures are given by,

$$\alpha_{P3BT/PS} = -0.300\times10^{-3} + (0.545 - 0.227\phi_{P3BT})/T \tag{10a}$$

$$\alpha_{P3HT/PS} = -0.719\times10^{-3} + (0.818 - 0.196\phi_{P3HT})/T \tag{10b}$$

$$\alpha_{P3OT/PS} = -0.770\times10^{-3} + (0.730 - 0.0475\phi_{P3OT})/T \tag{10c}$$

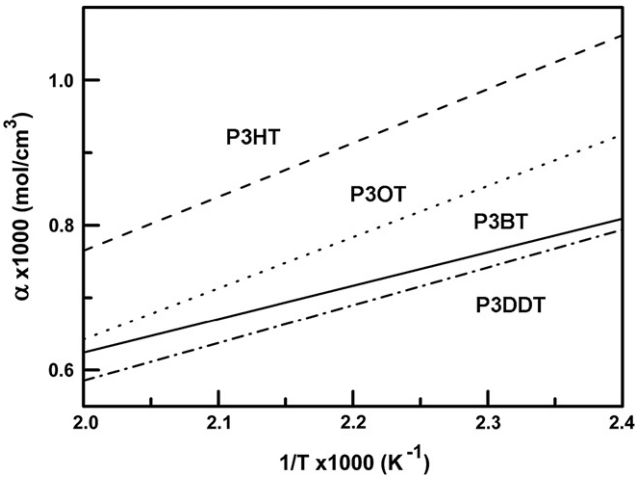

Fig. 3. Temperature dependence of α for four different P3AT/PS blends.

$$\alpha_{P3DDT/PS} = -0.458 \times 10^{-3} + (0.526 - 0.00812\phi_{P3DDT})/T \quad (10d)$$

where ϕ_{P3AT} is the volume fraction of P3AT in P3AT/PS blend. We used the specific volumes (in cm^3/g) of PS (0.952), P3BT (0.902), P3HT (0.915), P3OT (0.948), and P3DDT (1.03), respectively, which were measured at room temperature by densitometry (Mettler Toledo Ltd.).

Once the dependence of temperature and concentration of α is known for the blend system, the predicted binodal compositions (ϕ_2' and ϕ_2'') at a given temperature are obtained from Eqs. (6) and (7). The solid lines in Fig. 2a–d are the predicted binodal curves based on Eq. (10), from which all of the predicted binodal curves are in good agreement with measured turbidity curves.

Fig. 3 gives the temperature dependence of α for P3AT/PS blends at the critical composition ($\phi_{c,P3BT} = 0.37$; $\phi_{c,P3HT} = 0.39$; $\phi_{c,P3OT} = 0.51$; $\phi_{c,P3DDT} = 0.58$). Interestingly, the value α for P3AT/PS blends does not increase (or decrease) monotonically with n. With increasing n from 4 to 6, α increases, but, α decreases with further increase in n. Thus, the miscibility of P3HT/PS blend becomes the poorest, whereas that of the P3DDT/PS blend becomes the largest among four different alkyl side chains.

Now, we consider why the miscibility (or α) for P3AT/PS blends does not increase (or decrease) monotonically with increasing n. First, we estimate δ of each P3AT and PS by using three different group contribution methods [27], and the results are given in Table 2. When the difference between δ_{P3AT} and δ_{PS} becomes smaller, the better miscibility is expected. However, from the estimated δ of each P3AT and PS given in Table 2, any group contribution method could not explain the above experimental results.

Second, the effect of regioregularity on the miscibility can be considered. All the P3ATs employed in this study are neither complete regioregular nor regiorandom. The regioregularity was the smallest (75%) for P3OT and the largest (80%) for P3BT. Unfortunately, we could not have a very high value (for instance, 95% or more) of the regioregularity of P3AT because of small molecular weights of P3AT. However, we do not consider that the difference (at most 5%) in the regioregularity of P3AT does not change the phase diagram, although this effect is not completely excluded. Very recently, Jaczewska et al. showed that the value of δ of a regiorandom P3DDT having the 1:1 ratio of head-to-head (HH) to head-to-tail (HT) linkages was 16.9 $MPa^{1/2}$, which is much closer to δ of PS (17.8 $MPa^{1/2}$) than that (12.5 $MPa^{1/2}$) of a regioregular P3DDT with 98% HT linkage [12]. However, the HT regioregularity difference between these two P3DDTs in Ref. [12] was very large, namely, 98% of regioregular P3DDT versus 50% of regiorandom P3DDT.

Thus, to understand the interesting phase behavior of P3AT/PS depending on n, we estimate the χ between P3AT and PS via molecular simulations for two types (without and with annealing) of the configuration of 3AT monomers. Table 3 gives the values of χ

Table 2
Estimated solubility parameters (δ) of P3AT and PS by three group contribution methods.

δ ($MPa^{1/2}$)	P3BT	P3HT	P3OT	P3DDT	PS
Small	23.8	22.0	20.9	19.7	18.7
Hoftyzer & van Krevelen	18.6	18.0	17.6	17.2	19.1
Hoy	20.3	19.8	19.5	19.1	19.4

Table 3
The Flory-Huggins interaction parameter (χ) between P3AT and PS at 150 °C predicted by Monte Carlo method.

χ	Without annealing	With annealing
P3BT/PS	0.48	0.32
P3HT/PS	0.60	0.37
P3OT/PS	0.74	0.35
P3DDT/PS	1.49	0.20

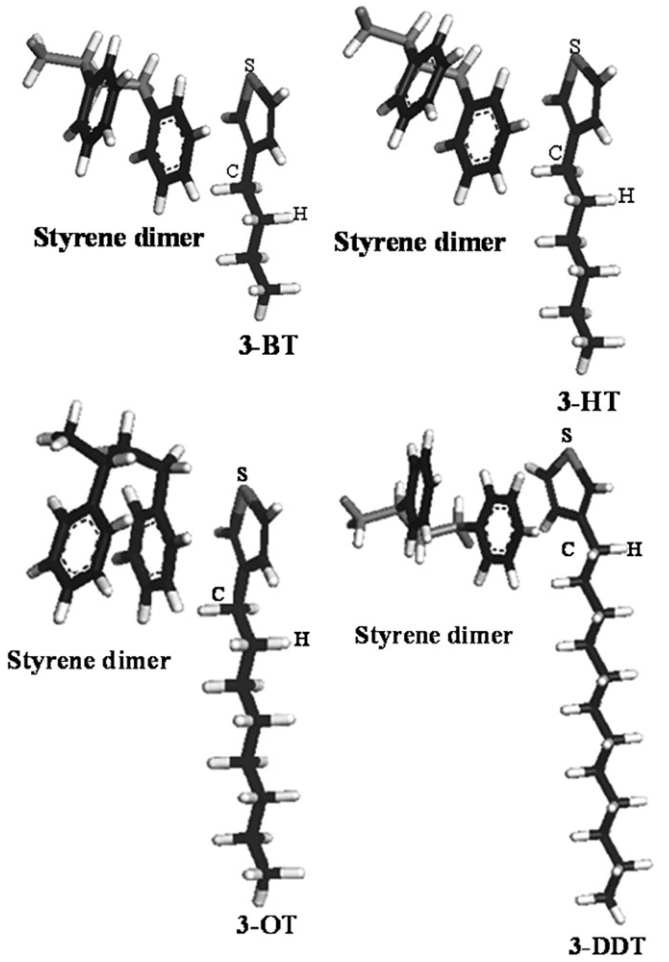

Fig. 4. The most probable configuations of unannealed 3AT and styrene generated by the MC simulation when all the 3AT monomers maintain the coplanar zigzag conformation.

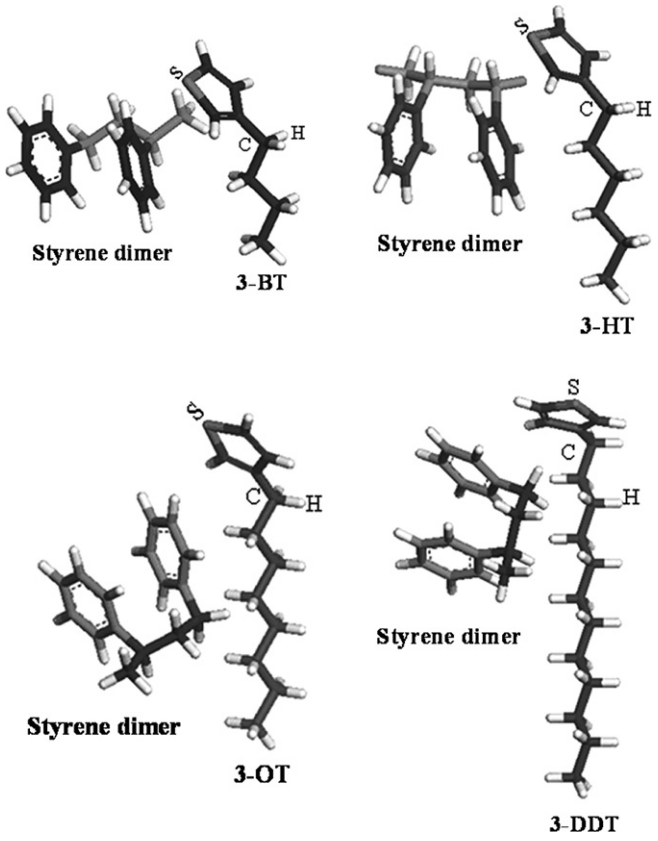

Fig. 5. The most probable configurations of the annealed 3AT and styrene generated by the MC simulation.

between four 3AT monomers and styrene dimers at 150 °C without and with the annealing process of MD, respectively. Without annealing, when styrene and 3AT approach each other, the most probable conformation of styrene chains would be that the benzene rings in the styrene are packed perpendicular to the coplanar plane of the thiophene ring and the alkyl side chain, as shown in Fig. 4. Thus, the backbone of styrene was forced to be located away from the side chain of the 3AT, which results in the increased χ with the increase of the alkyl side chain length.

On the other hand, both the thiophene ring and the alkyl side chains in the P3AT do not need to maintain the coplanar conformation after the annealing, as shown in Fig. 5, where the most probable configurations of the styrene and annealed 3AT monomer in the blend are displayed. In this situation, the benzene rings in styrene could be attracting each other to get closer to the thiophene ring, and the degree of the repulsion associated with the alkyl side chain was not as much as that in the coplanar conformation. Furthermore, with increasing n, the carbon backbone of styrene was attracted by the alkyl side chain of 3AT, which decreases the incompatibility of 3AT and styrene.

In other words, the attraction between the benzene rings in the PS and the thiophene rings in the P3AT enables the PS and P3AT chains to be close to each other because of similar π-conjugated electrons in the both rings. Thus, the benzene rings suffer a larger degree of the repulsion associated with the longer alkyl side chains in the P3AT, which results in the increase of χ with increasing value of n. On the other hand, since the attraction between the carbon backbone of PS and the alkyl side chain of P3AT, resulting from similar hydrophobic natures of the hydrocarbons, increases with increasing n, χ decreased. Therefore, χ between P3AT and PS was first increased and then decreased with increasing n. The predicted maximum in χ for P3HT/PS blend is in good agreement with the results given in turbidity measurement.

5. Conclusions

We have shown that all of the P3AT/PS blends exhibited UCST type phase behavior regardless of values of n. Interestingly, the UCST at a given molecular weight did not monotonically increase (or decrease) with n. Instead, the miscibility of P3HT/PS blend became the least, while the P3DDT/PS blend showed the best miscibility among the four P3AT/PS pairs. This interesting phase behavior depending on n was successfully illustrated via the combination of Monte Carlo and molecular dynamics simulation.

Acknowledgment

This work was supported by the National Creative Research Initiative Program supported KOSEF. C. I. H. acknowledges the financial support of the National Science Council of the Republic of China through grant NSC 97-2628-E-002-001-MY3.

References

[1] Wang G, Swensen J, Moses D, Heeger AJ. J Appl Phys 2003;93:6137.
[2] Sirringhaus H. Adv Mater 2005;17:2411.
[3] Panzer MJ, Frisbie DD. Adv Funct Mater 2006;16:1051.
[4] Li B, Sauve G, Iovu MC, Jeffries-El M, Zhang R, Cooper J, et al. Nano Lett 2006;6:1598.
[5] McQuade DT, Pullen AE, Swager TM. Chem Rev 2000;100:2537.
[6] Padinger F, Rittberger RS, Sariciftci NS. Adv Funct Mater 2003;12:85.
[7] Reyes-Reyes M, Kim K, Carroll DL. Appl Phys Lett 2005;87:083506.
[8] Li G, Shrotriya V, Huang J, Yao Y, Moriarty T, Emery K, et al. Nat Mater 2005;4:864.
[9] Kim JY, Lee K, Coaters NE, Moses D, Nguyen T, Dante M, et al. Science 2007;317:222.
[10] Goffri S, Müller C, Stingelin-Stutzmann N, Breiby DW, Radano CP, Andreasen JW, et al. Nat Mater 2006;5:950.
[11] Lu G, Tang H, Qu Y, Li L, Yang X. Macromolecules 2007;40:6579.
[12] Jaczewska J, Raptis I, Budkowski A, Goustouridis D, Raczkowska J, Sanopoulou M, et al. Synth Met 2007;157:726.
[13] Jaczewska J, Budkowski A, Bernasik A, Moons E, Rysz J. Macromolecules 2008;41:4802.
[14] Levon K, Chu E, Ho KS, Kwei TK, Mao J, Zheng WY, et al. Polym Sci Polym Phys 1995;33:537.
[15] Vicente L, Soto C, Pacheco-Sanchez H, Hernandez-Trujillo J, Martinez-Magadan JM. Fluid Phase Equilib 2006;239:100.
[16] Kuo M, Yang H, Hua C, Chen C, Mao S, Deng F. Chem Phys Chem 2004;5:575.
[17] Patnaik S, Pachter R. Polymer 2002;43:415.
[18] Fan CF, Olafson BD, Blanco M, Hsu SL. Macromolecules 1992;25:3667.
[19] Kellogg RM, Schaap AP, Harper ET, Wynberg H. J Org Chem 1968;33:2902.
[20] Liu J, Sheina E, Kowalewski T, McCullough RD. Angew Chem Int Ed 2002;41:329.
[21] Liu J, Loewe RS, McCullough RD. Macromolecules 1999;32:5777.
[22] Chen TA, Wu X, Rieke RD. J Am Chem Soc 1995;117:233.
[23] Lin JL, Roe RJ. Macromolecules 1987;20:2168.
[24] Stobl GR, Bendler JT, Kambour RP, Schultz AR. Macromolecules 1986;19:2683.
[25] Koningsveld R, Onclin MH, Kleintjens LA. In: Solc K, editor. Polymer compatibility and incompatibility. MMI press; 1982.
[26] Koningsveld R, Stockmayer WH, Nies E. Polymer phase diagram. Oxford University Press; 2001.
[27] Brandrup I, Immergut EH, Grulke EA, editors. Polymer handbook. 4th ed. New York: John Wiley & Sons; 1999.